Chapter 11

Harvesting Plasmonic Excitations in Graphene for Tunable Terahertz/Infrared Metamaterials

Yuancheng Fan, Fuli Zhang, Quanhong Fu and Hongqiang Li

Additional information is available at the end of the chapter

http://dx.doi.org/10.5772/64361

Abstract

In this chapter, we focus on the development on tunable terahertz/infrared metamaterials enabled with plasmonic excitations in graphene micro-/nanostructures. We aimed the issue that high loss in the plasmonic excitations of graphene limits the performance of graphene's ability in manipulating light. We show the enhancement of light-graphene interactions by employing plasmonic metamaterial design for proper plasmonic excitations, and coherent modulation on optical fields to further increase the bonding of light field for boosted plasmonic excitations. The enhanced plasmonic excitations in graphene provide the possibility of practical applications for terahertz and infrared band graphene photonics and optoelectronics.

Keywords: graphene, plasmonics excitations, tunable metamaterials, terahertz, infrared, surface conductivity

1. Introduction

There have been numerous reports on scientific advances in graphene, a first realistic two-dimensional (2D) material with carbon atoms arranged in a hexagonal lattice. Since its first exfoliation from graphite by Geim and Novoselov [1, 2], graphene stimulated and led the research upsurge in two-dimensional materials [3, 4]. It is attractive for myriad applications that profits from its high electronic mobility (25,000 cm^2/V^{-1} s^{-1}) [5], exceptional mechanical strength (~1.0 TPa) [6], and thermal conductivity [7]. It has also been widely investigated for potential applications in photonics and optoelectronics [8–10]. Graphene exhibits much stronger binding of surface plasmon polaritons [11–16], and the Dirac fermions in graphene

provide ultra wideband tunability in optical response through electrostatic field, magnetic field, or chemical doping [15–20]. All these are good for dynamical control on optical signals. However, there are still some challenges in developing graphene photonics for practical applications. One of them is that graphene is almost transparent to optical waves due to the relatively low carrier concentrations in the monolayer atomic sheet; this might be useful for some cases, for example, for the transparent electrodes, but strong light-matter interactions is the most crucial part for practical optical applications. Boosting the light-matter interaction in graphene is one important issue to address to take further advantage of graphene in optical devices or systems, for example, to realize functionality such as optical insulator similar to gapped graphene [21–23] for nanoelectronics, which is essential for myriad applications in all-optical systems and components of much miniaturized optical circuits [24–26]. It is important to take effectual strategies to improve the light-graphene interactions.

1.1. Plasmonic metamaterials

Artificially engineered microstructures, that is, the plasmonic metamaterial and photonic crystals, are well-known platforms for the enhancement of light-matter interactions [27–29]. Optical absorption enhancement in graphene had been demonstrated in a photonic crystal nanocavity for high-contrast electro-optic modulation, at the regime of critical coupling with photonic crystal-guided resonance, and in photonic crystals for broadband response [30–34]. And in the meanwhile, plasmonic metamaterials [35–42] with even miniaturized elements are promising for the manipulation of light at the deep subwavelength scale by making use of the plasmonic excitations. Especially a kind of metamaterials with a single 2D function layer, named as metasurface [43–49], has been intensively studied in recent years for various possibilities to manipulate light peculiarly. The metasurface is naturally connected to the 2D graphene for the following: (i) changing conversional plasmonic material-metal with graphene will provide frequency-agile responses and make the metasurface even more subwavelength and (ii) the light-graphene interactions can be significantly enhanced in an atomically thin graphene metasurface. Optical absorption enhancement has been studied in graphene nanodisks, in which periodic graphene disks are placed on a substrate or a dielectric layer with metallic ground, the plasmonic excitations in the structure resulting in the complete absorption of incident light. Graphene micro-/nanoribbons, split ring resonators, mantles, nanocrosses, and photonic crystals have also been exploited for controlling terahertz and infrared light.

1.2. Coherently modulated light-matter interactions

Another strategy that was proposed recently to remarkably improve the light-matter interaction is the coherent modulation technique, which is based on the coherence of optical fields. The coherence of laser made it unique in modern optics and photonics. A coherent perfect absorber (CPA), also called anti-laser, was recently proposed [50] and demonstrated [51] in a Si-resonator. The coherent absorption comes from the phase modulation on light fields. Since the first proposal, relevant coherent modulation-assisted processes have attracted considerable research interests with various photonic structures [52–58], for example, laser absorber and

http://dx.doi.org/10.5772/64361

symmetry breaking in PT-symmetric optical potentials and strongly scattering systems, unidirectional invisibility in PT-symmetric periodic structures, and perfect mode (polarization or morphology) conversions. It has been proven that coherently modulated optical field provides additional localization of the light within artificially engineered microstructures, including both the photonic crystals and plasmonic metamaterials, to further boost light-matter interactions.

In this chapter, we summarize our recent studies on the excitation of electric/magnetic plasmonic modes in graphene structures [59, 60], and their synergic action with the coherently modulated optical fields that provide strong interaction between graphene and light for practical and tunable terahertz/infrared metamaterials or metasurfaces [61, 62].

2. Tunable plasmonic excitations in graphene metamaterials

2.1. Optical conductivity of graphene

The optical response of a monolayer graphene can be described with the complex surface conductivity in the local-random phase approximation (RPA) approximation as

$$\sigma(\omega)=\frac{2e^2T}{\pi\hbar}\frac{i}{\omega+i\tau^{-1}}\log\left[2\cosh\left(E_F/2k_BT\right)\right] + \frac{e^2}{4\hbar}\left[H\left(\omega/2\right)+\frac{4i\omega}{\pi}\int_0^{\infty}\frac{H\left(\varepsilon\right)-H\left(\omega/2\right)}{\omega^2-4\varepsilon^2}d\varepsilon\right]\Bigg\}, \tag{1}$$

with $H(\varepsilon)=\frac{\sinh(\hbar\varepsilon/k_BT)}{\cosh(E_F/k_BT)+\cosh(\hbar\varepsilon/k_BT)}$, ω is the angular frequency of the incoming light wave, e is the electron charge, $\hbar$ is the reduced Planck constant, k_B is the Boltzmann constant, and T is the temperature. τ is a phenomenological relaxation time representing the scatterings in graphene or the quality of graphene sample, E_F is the Fermi energy away from the Fermi surface.

Figure 1 shows the surface conductivity of a monolayer graphene (Fermi level: 0.1 eV) at 0 K. We can see that the total conductivity of the graphene includes two parts: (i) contribution from the intraband transition (blue), the response is similar to Drude dispersive metals; and (ii) contribution from the interband transition (green), with near nondispersive real conductivity at frequencies higher than double Fermi level. For that graphene is interesting for dynamically controlled photonic applications, we plot the surface conductivities under different Fermi levels (from 0.06 to 0.14 eV) in **Figure 2**; we can see from the figure that the conductivity of graphene can be s-tuned by changing the Fermi level, especially the low-frequency Drude-like response. The tunable Drude-like metallic behavior has received intensive attention in the past years, and this chapter focuses on the tunable plasmonic excitations in graphene at terahertz/infrared frequencies.

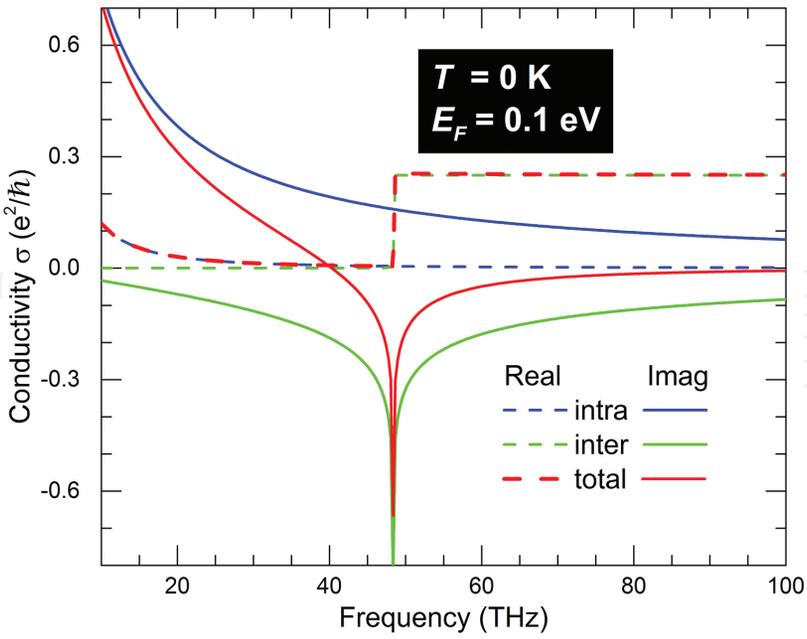

Figure 1. Complex surface conductivity of a monolayer graphene (Fermi level: 0.1 eV) at 0 K.

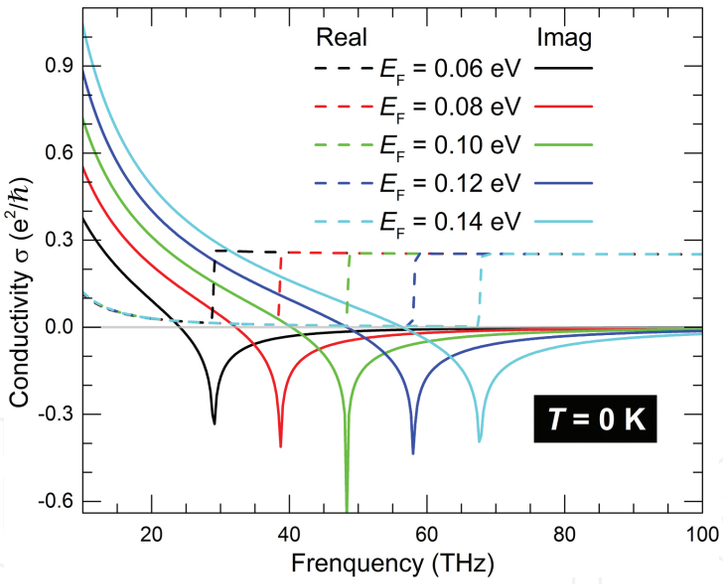

Figure 2. Tunable surface conductivity of a monolayer graphene (Fermi level: from 0.06 to 0.14 eV) at 0 K.

2.2. A comparative study on the plasmonic excitations in graphene split ring resonators (SRRs)

We proposed to enhance infrared extinction and absorption in a monolayer graphene sheet by patterning split ring resonators, a kind of basic structure in the design of plasmonic metamaterials. By introducing asymmetric split ring resonators (ASRRs) into the monolayer graphene sheet, we excited both fundamental magnetic mode and electric mode, and the

contributions on the enhancement of infrared extinction and the absorption of these two modes are comparatively studied. The designed periodic SRR-patterned graphene metamaterial is shown in **Figure 3**, the rings are with width a=2.5 μm and the lattice constant of the square lattice is P=3.0 μm, the gap size of SRR is g=0.6 μm. We note that the line width w of the ring and the gap center position ($\delta$with respect to the center of the ring) are parameters that can significantly influence absorption/extinction properties of the graphene metamaterial.

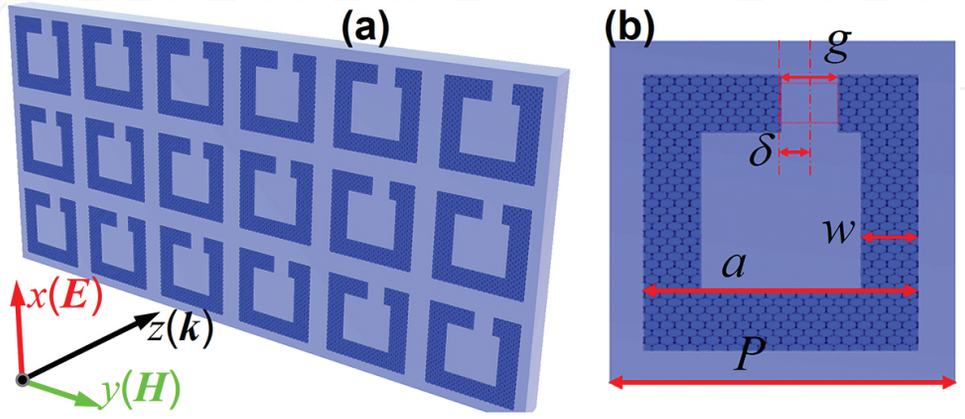

Figure 3. (a) Schematic of the SRR-patterned monolayer graphene sheet and corresponding electromagnetic excitation configuration (the polarization direction is along the x-axis). (b) A unit cell of the SRR-patterned graphene sheet. Geometric parameters are denoted by black letters.

In calculations, the graphene sheet was approximately treated as optical interface with complex surface conductivity, since a one-atom-thick graphene sheet is sufficiently thin compared with the concerned wavelength; the complex surface conductivity can be well described by a Drude model as $\sigma = e^2 E_F / (\pi\hbar^2) * i / (\omega + i\tau^{-1})$, especially at low frequencies and heavily doped region, where E_F=0.5 eV is the Fermi energy away from Dirac point, and $\tau = uE_F / ev_F^2$ is the relaxation rate with $\mu = 10^4 \mathrm{cm^2 V^{-1} s^{-1}}$ and $v \approx 10^6$m/sbeing the mobility and Fermi velocity, respectively. The Fermi level can be easily controlled by electrostatic doping via tuning charge-carrier density.

First, we set δ=0.45 μm≠0, which introduces symmetry breaking in SRRs. It is known that both the electric mode and the fundamental magnetic mode can be excited for normal incidence in the ASRR metamaterial [63–65]. It can be seen from **Figure 4** that there are two transmission dips on the curve. The transmission and reflection coefficients of the electric-field magnitude of the x-polarized incident wave are defined as $t_{ix} = |E_i^{\mathrm{Tran}} / E_x^{\mathrm{Inc}}| (i = x, y)$, and $r_{ix} = |E_i^{\mathrm{Ref}} / E_x^{\mathrm{Inc}}|$), in which E_x^{Inc} is the field of incident wave, and E_i^{Tran} and E_i^{Ref} are the field of transmitted or reflected waves. We confirmed that (through numerical simulation) these two dips correspond to fundamental plasmonic resonances: magnetic mode and electric mode. The electric resonant mode at 3.96 THz is well excited. The magnetic mode at 1.99 THz is with a very shallow dip in the transmission curve, which indicates that the graphene ASRR is weakly excited. When comparing the resonant strength with resonant dips, it is clear that the electric resonant mode is stronger in responding the incident field, and it shows better extinction and

absorption compared with the magnetic mode. We believe that this is because the graphene's low-carrier concentration leads to the weak capturing on optical fields. The electric dipolar mode is easier to excite, because to excite the electric mode capturing the incident field into a current loop is not required. We also notice that the polarization transformation $t_{yx}=r_{yx}\neq 0$, which is the radiation from the induced surface current on the graphene ASRRs. This polarization conversion will also influence the optical extinction and absorption of the x-polarized incident waves. The optical extinction and absorption with respect to x-polarized incident wave are defined as $E=1-|t_{xx}|^2$ and $A=1-|t_{xx}|^2-|r_{xx}|^2-|t_{yx}|^2-|r_{yx}|^2$for considering the polarization conversion.

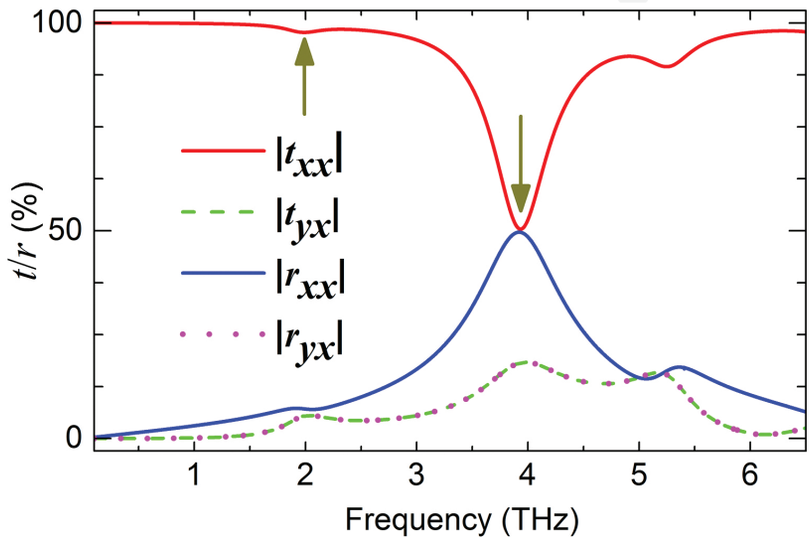

Figure 4. Transmission (t) and reflection (r) coefficients with respect to the x-polarized incident wave of ASRRs-patterned graphene sheet (gap position $\delta=0.45$ μm and line width of graphene ASRR $w=0.5$ μm).

We investigate the influences of geometric parameters on the optical extinction and absorption of the ASRR graphene metamaterial. **Figure 5** shows resonant frequencies of the electric mode and the magnetic mode, and the extinction and absorption at resonant frequencies for graphene metamaterial with different line widths. The extinction on the resonance for both the electric mode and the magnetic mode rises as the line width becomes wider, and the extinction of the electric resonance is nearly one order higher than that of the magnetic resonance. We can see that the extinction can be efficiently boosted at the frequency of electric resonance, for example, the optical extinction of about 87% at a wavelength of 58.5 μm is achieved.

Then, we investigate the influence of symmetry (of the SRR structure) on the optical extinction and absorption. We find that the resonant frequency of the electric mode almost did not shift when changing the asymmetric parameter, and the enhanced extinction and absorption of the symmetric SRR ($E=81\%$, $A=49\%$) is higher than that of the ASRR ($E=75\%$, $A=43\%$). Then, we study comparatively the extinction and absorption in symmetric ($\delta=0$) and asymmetric ($\delta=0.45$ μm) graphene SRRs. We find that the symmetric SRR is better than ASRR for

http://dx.doi.org/10.5772/64361

the enhancement of extinction and absorption in a monolayer of graphene. A maximum extinction of about 90% (w=0.8 μm) and a maximum absorption of 50% (w=0.4 μm) can be achieved in a symmetric SRR graphene metamaterial. Since only an electric resonance is excited in the symmetric SRR structure, and there exists no polarization conversion, the enhancement on the extinction and absorption can be understood simply as follows: First, the SRRs trap optical field that shines on graphene according to their receiving ability. Then, the trapped field is redistributed through an absorbing channel and a radiating channel (including both the forward and backward radiation). We note that the receiving or radiating ability of the graphene SRRs and trapped ratio with respect to the incoming energy are two key characters in this process, and these two aspects are both strongly connected to the line width of the graphene SRRs. On the one hand, the radiating property can be significantly influenced by changing the line width since we know that a thin dipole possesses better radiation. On the other hand, the line width determines directly the graphene area ratio to the whole unit cell and thus remarkably modulates the trapped ratio to the incident light as well as the absorption in the graphene metamaterial. The electric resonance and dissipation of the graphene will compete for an optimized absorption, while for the extinction the incident light is more likely to be scattered for SRRs with wider line widths, which contributes to an incremental optical extinction.

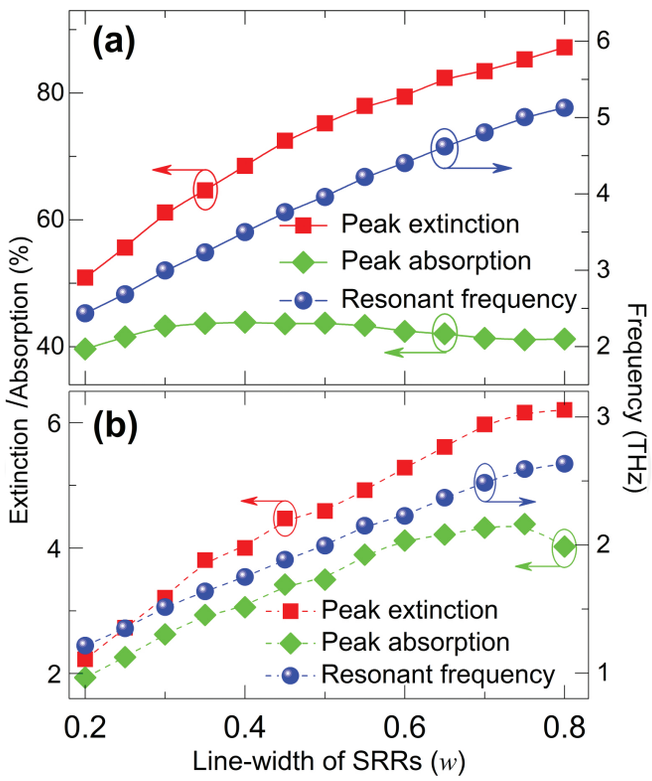

Figure 5. Resonant frequency (blue sphere), extinction (red square), and absorption (olive diamond) at resonant frequencies of the ASRR (with δ=0.45 μm)-patterned monolayer graphene sheet with respect to different line width w for electric mode (solid) (a) and magnetic mode (dashed) (b).

2.3. Electric plasmonic excitation in graphene cut-wires and physics of a maximum 50% absorption in graphene metamaterials

We have found that the electric dipolar mode is stronger in enhancing light-graphene interactions at terahertz frequencies compared to the magnetic mode and other higher-order modes. As the simplest structure that supports electric dipolar excitation, cut-wire is essential in designing plasmonic metamaterials. It has been widely adopted for exploring fundamental physics as well as novel functionalities, such as plasmon-induced transparency, polarization manipulations, and optical antennas. We suggested a tunable metasurface by exploiting a monolayer graphene patterned in a cut-wire array. We mainly focused on the strengthening of graphene's terahertz response by the electric dipolar excitation of the basic cut-wire structure and the influences of the graphene qualities. A 50% maximum absorption at the electric dipolar mode is confirmed by the extraction of effective surface conductivities of a cut-wire array of the theoretical and experimental graphene. Systematic investigations to the graphene metasurface by changing values of graphene sample between two sets of well-known experimental data, that is, Li et al. data [18] and Yan et al. data [10], respectively, show that optical response of the graphene cut-wire-based metasurface can be tuned substantially in terahertz frequencies.

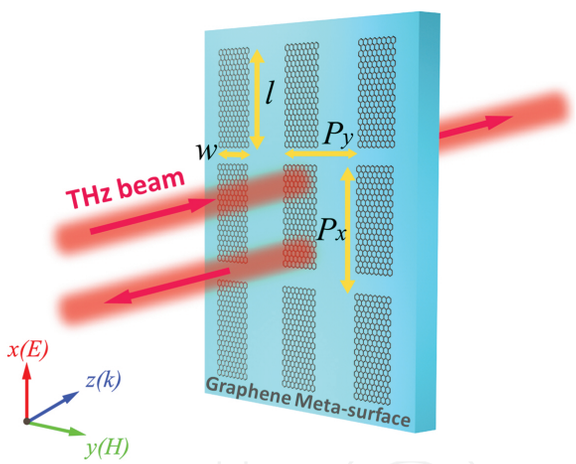

Figure 6. Schematic of the single-layer graphene cut-wire structure together with the corresponding excitation configuration: *x*-polarized incident light is propagating along the *z*-axis. Geometric parameters are denoted by black letters.

Figure 6 shows the schematic of the proposed tunable graphene metasurface. The meta-atoms, that is, graphene cut-wires, are periodically arranged in *xy*-plane with lattice constants P_x =6 μm and P_y =3 μm. The length and width of the cut-wire meta-atoms are l and w, respectively. In the setup, the THz beam, with electric field polarized along the *x*-direction, normally illuminates graphene metasurface along the *z*-axis.

We first took E_F =0.5 eV for the graphene, and the width of the wire w =0.7 μm. The changes of the resonant frequency and the peak absorption for the fundamental resonance caused by the increase of the cut-wire length (l) are plotted in the inset of **Figure 7(a)**. We see that the resonant frequency dropped dramatically to a lower frequency while the peak absorption found its

http://dx.doi.org/10.5772/64361

maximum of 50% around 5.0 μm. **Figure 7(a)** presents the spectra of transmission (T), reflection (R), and absorption (A) spectra for the case of graphene cut-wire metasurface with the length of the wire l =5.0 μm. We can see an obvious resonance around 3.30 THz. From our investigation on the local field and current distributions, the resonance was confirmed to be an electric dipolar mode. It is well known that the resonance frequency of cut-wires changes with the length of the corresponding meta-atom. However, it is found that the width of cut-wires also plays an important role in determining the electromagnetic (EM) properties of graphene metasurface. Then, we specifically focus on studying the influence of w to the optical response of the cut-wire-array metasurface, by setting the length l at a constant value 5.0 μm. The absorption spectra of cut-wires with different line width show the influence of line width to the terahertz performance of graphene cut-wire array; we find that the resonant frequency of the electric mode shows a monotonous blue shift as we increase the line width w. On the other hand, we also notice that there exists an inflection for the absorption enhancement, which runs up to the maximum under w =0.7 μm at around 3.30 THz. The simple cut-wire structure confirms that the 50% maximum absorption enhancement still holds for the excitation of electric dipolar mode in a graphene sheet [59].

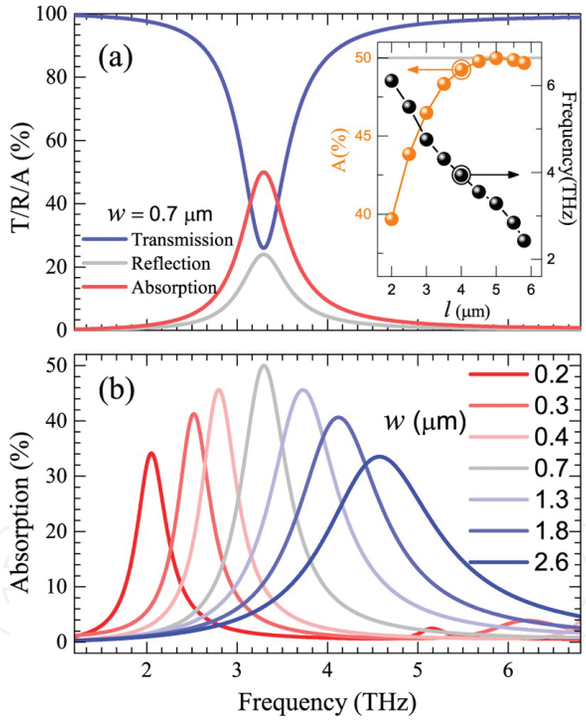

Figure 7. (a) Transmission, reflection, and the absorption of a graphene cut-wire array; the inset shows resonant frequencies and the peak absorptions for cut-wires with different lengths. (b) The absorption spectra for graphene cut-wire arrays with different cut-wire widths: the resonant spectra show a blue shift (from red to blue) regarding the increase of the widths.

Actually, the 50% maximum absorption of graphene metasurface can be understood simply with a transfer matrix study on a conductive sheet: since the graphene cut-wires are of deep subwavelength, we can neglect high-order scatterings of graphene metasurface, for that the

unit cells of graphene metasurface are all of deep subwavelength, then we have the absorption (A) of a free-standing metasurface (described as a conductive sheet with effective complex conductivity σ)

$$\begin{aligned} A &= 1-|r|^2-|t|^2 \\ &= 1-\left|\frac{\sigma\eta_0}{2+\sigma\eta_0}\right|^2-\left|\frac{2}{2+\sigma\eta_0}\right|^2 \\ &= \frac{4}{\left(\left[4+\left(\sigma_i\eta_0\right)^2\right]/\sigma_r\eta_0\right)+\sigma_r\eta_0+4} \\ &\le \frac{1}{2} \end{aligned} \tag{2}$$

where η_0 represents the characteristic impedance of vacuum, r and t are the complex scattering coefficients, and σ_r and σ_i are the real and imaginary parts of σ, respectively. We can find that the absorption receives the maximum, that is, 50%, when $\sigma_r\eta_0$=2 and σ_i=0 (or simply $\sigma\eta_0$=2).

The retrieval method [66, 67] for the calculation of effective EM parameters from measured r and t coefficients provides a very intuitive route to understand the EM properties of metamaterials. Here, we applied a recently proposed retrieval method for sheet materials [68] to understand the THz response of the metamaterial designs; the sheet retrieval method is suitable for our 2D graphene structure. The effective electric surface conductivity $\sigma_{\parallel}^{e}$ can be obtained from the complex scattering coefficients

$$\sigma_{\parallel}^{e} = \frac{2}{\zeta}\left(\frac{1-r-t}{1+r+t}\right) \tag{3}$$

with ζ representing the wave impedance. The extracted complex surface conductivity of the graphene metasurface for the case of w=0.7 μm is shown in **Figure 8**. The resonant response around 3.30 THz can be seen on the effective electric conductivity spectrum, which is the proof of the excitation of electric dipolar mode. So far, we have investigated the graphene metasurface with the theoretical data, that is, the Drude weight and the collision frequency are α=58.86 GHz/Ω and γ=2 THz. We then consider the metasurface with graphene data from experimental measurements, that is, the Yan et al. graphene with α=76.0 GHz/Ω and γ=9.8 THz THz. The same procedure for studying the influence of w was performed and the 50% maximum absorption occurs when w=2.6 μm. The retrieved electric conductivity for Yan et al. graphene metasurface is presented in **Figure 8**, the electric resonance is shifted to 5.06 THz for this case. It is interesting that the amplitudes of the effective conductivity of the metasurfaces are nearly the same (as indicated in **Figure 8**). We also see from the figure that $\sigma\eta_0$=2 is almost fulfilled for the maximum 50% absorption at the resonant frequencies.

http://dx.doi.org/10.5772/64361

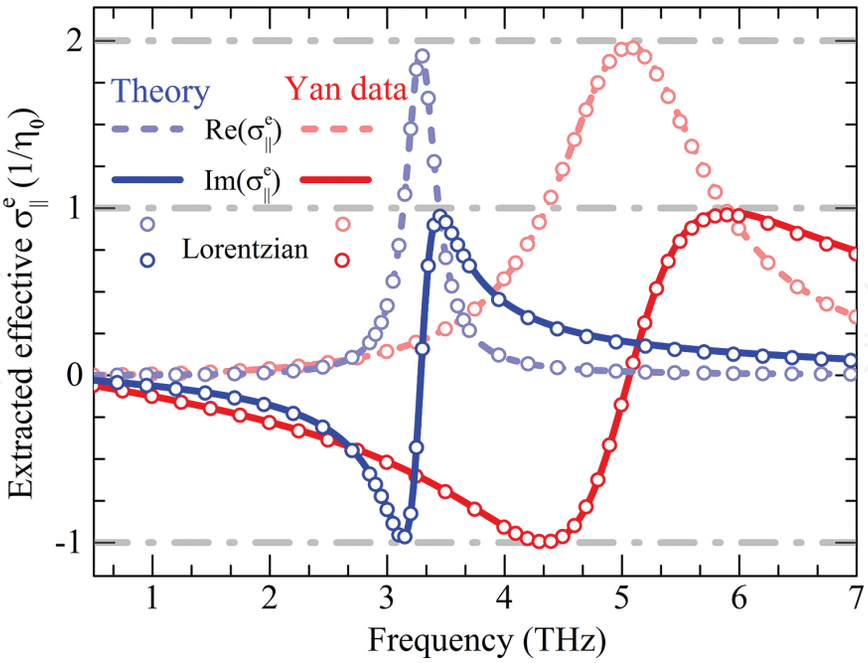

Figure 8. Extracted effective surface conductivities for graphene cut-wire arrays with theoretical graphene data and Yan et al. graphene data, respectively. Lorentzian fittings of the resonant conductivity responses are plotted on the extracted curves.

Since the effective electric surface conductivity of the graphene metasurface shows a Lorentz response, we used a Lorentzian function to fit the conductivity for quantitative descriptions of the electric resonances

$$\sigma_{\parallel}^{e} = \frac{i\kappa f 2}{f^2 + i\Gamma f - f_r^2} - i\beta f \tag{4}$$

where f_r is the frequency of resonance, Γ represents the damping, κ is a constant measuring coupling, and β characterizes the background polarization. The fitted Lorentz factors of the theoretical graphene data case are f_r=3.30 THz, Γ=315.0 GHz, and κ=606.4 GHz, while for the Yan et al. graphene data case these parameters are f_r=5.06 THz, Γ=1554.0 GHz, and κ=3048.1 GHz. We found two connections from the fitted Lorentz parameters: $\Gamma_2/\Gamma_1 \approx \gamma_2/\gamma_1$ and $\kappa_1/\Gamma_1 \approx \kappa_2/\Gamma_2$ (in which subscripts 1 and 2 denote the cases with theoretical and Yan et al. graphene data). These two relations imply the following: (i) the damping factor of plasmonic excitation of the graphene metasurface is determined by the collision frequency in graphene; and (ii) graphene metasurfaces with the same absorption (50% maximum absorption in our study) have nearly the same resonant amplitudes—κ/Γ.

To further investigate the graphene metasurface with different surface conductivities, we comparatively studied the graphene metasurface by changing the values of α and γ between that of the two sets of well-known experimental data, that is, Li et al. graphene (α=19.9 GHz/Ω, γ=29.4 THz) and Yan et al. graphene. The line width of cut-wires w is set as 2.6 μm for the

discussions in this section. The false-color maps of the extracted electric surface conductivity are plotted in **Figure 9(a)** and **(b)**, respectively. We change the parameters of graphene from the Li et al. data (denoted as 1) to the Yan et al. data (denoted as 3) in two steps: decreasing collision frequency and increasing Drude weight (2 represents a hypothetic graphene data with $\alpha = 19.9\ \mathrm{GHz}/\Omega$ and $\gamma = 9.8\ \mathrm{THz}$). From $1 \rightarrow 3$, it can be seen that the electric dipolar resonance changed considerably as we improved the quality of graphene (from the Li et al. data in 2008 to Yan et al. data in 2012), which can be confirmed quantitatively from **Figure 9(c)**, in which we plotted the fitted resonant frequencies and *Q*-factors (f_r / Γ) of the studied graphene metamaterial: (i) the resonant frequency maintains nearly the same when decreasing the collision frequency; however, the changing of the damping frequency makes the *Q*-factor to increase linearly; (ii) the damping frequency maintains when increasing the Drude weight; however, the blue shift of the resonant frequency makes the *Q*-factor to increase continuously during the increase in the Drude weight.

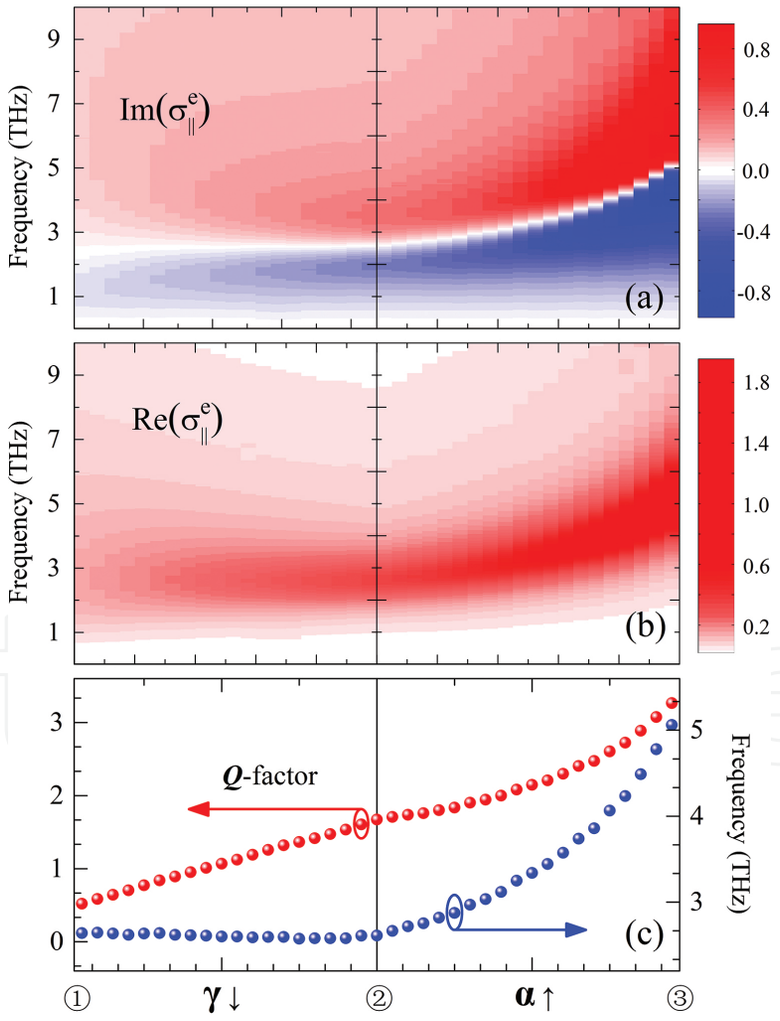

Figure 9. Spectra of imaginary (a) and real (b) parts of extracted effective surface conductivities as a function of the graphene Drude weight α and the collision frequency γ. (c) *Q*-factors and resonant frequencies of graphene cut-wire arrays with different Drude weights and collision frequencies.

http://dx.doi.org/10.5772/64361

3. Graphene plasmonic excitations in coherently modulated optical fields

3.1. A monolayer graphene as a tunable terahertz CPA

We suggest enhancing the terahertz absorption with the technique of coherent modulation in an unstructured and nonresonant monolayer graphene. We found that the quasi-CPA frequency, at which the formation condition of CPA is fulfilled, does exist in the terahertz band for suspending graphene. The scattering of coherent beams can be perfectly suppressed with proper coherent modulation on the input beams. In our theoretical study, a layer of graphene is free standing in vacuum, and it is illuminated by two counter-propagating and coherently modulated input beams ($I_{\pm}$), $O_{\pm}$ are the respective output magnitudes.

In the monolayer graphene system, the complex scattering coefficients ($O_{\pm}$) can be related to the two input beams ($I_{\pm}$) through a scattering matrix, S_g, which is defined as

$$\begin{pmatrix} O_+ \\ O_- \end{pmatrix} = s_g \begin{pmatrix} I_+ \\ I_- \end{pmatrix} = \begin{pmatrix} t_+ & r_- \\ r_+ & t_- \end{pmatrix} \begin{pmatrix} Ie^{i\phi_+} \\ Ie^{i\phi_-} \end{pmatrix} \tag{5}$$

where $t_{\pm}/r_{\pm}$ are the scattering elements of the forward (I_+) and backward (I_-) beams; the scattering matrix can be simplified for that the system is of reciprocity and spatial symmetry. We consider only phase modulation on the coherent input beams for simplicity, then the two input beams are of equal amplitude I; the amplitude of the output beams would be

$$\left|O_+\right| = \left|O_-\right| = \left|tIe^{i\phi_+} + rIe^{i\phi_-}\right| \tag{6}$$

In a terahertz coherent perfect absorber, the coherent modulation of the input beams performance is required to inhibit the scatterings and thus stimulate the complete absorption of coherent terahertz beams, which requires $tIe^{i\phi_+}=rIe^{i\phi_-}$, we get the necessary condition for acquiring CPA performance: $|t| = |r|$.

In calculations, the graphene sheet can be considered as an optical interface described by complex surface conductivity (σ). Reflection and transmission coefficients of forward- and backward-propagating light through the graphene can be driven with the assistance of Ohm's law. The scattering elements t and r at the normal incidence are given by

$$t = \frac{2}{2 + \sigma\eta_0}, \tag{7}$$

$$r = \frac{\sigma\eta_0}{2 + \sigma\eta_0}, \tag{8}$$

where $\eta_0$is the wave impedance of free space. From these equations, we can give the condition for coherent perfect absorption:

$$|\sigma\eta_0| = 2 \tag{9}$$

In the work, we also found that the CPA based on a monolayer graphene is of angularly sensitivity, which is good for wide angular tunability. For oblique incidence, we should consider both *s*- and *p*-polarized modes; it is found with a transfer matrix formalism that the quasi-CPA frequency splits into two frequency branches for the two polarizations: the CPA of *s*-polarization has a blue shift compared to the normal incident case, while the CPA of *p*-polarization has a red shift compared to the normal incident situation. The two bands together covered a wide frequency range.

The charge-carrier density and thus the Fermi level can be easily changed through electrostatic doping, which makes graphene promising for wide-tunable and broadband optoelectronic and photonic applications. With the increase in the electrostatic doping, we get higher charge-carrier concentration and thus higher Fermi energies, and we found a blue shift of the quasi-CPA frequency. This process can be understood as follows: the Drude weight of graphene (with higher carrier concentration) becomes higher, or we can say the graphene is with reenforced metallicity, which will have more scattering, then the reflection will be increased and the transmission will be decreased, and the quasi-CPA point will show a blue shift.

3.2. Graphene metamaterial interaction with coherent-modulated optical field as a tunable infrared CPA

The discussed suspending monolayer graphene CPA is physically based on the intrinsic Drude response of graphene, which is realizable only in the few-terahertz range with achievable graphene samples. And then we exploited the possibility of coherent perfect absorption at infrared frequencies. We designed a graphene nanoribbon-based metasurface and found that quasi-CPA frequencies, which is the necessary formation condition of coherent absorption, do exist in the mid-infrared regime for properly designed graphene nanoribbon arrays. The scattering of coherent beams can be perfectly suppressed at the quasi-CPA frequencies with proper phase modulations on the input beams. For the case with two crosses on the transmission and reflection spectra, we can achieve coherent perfect absorption at the two quasi-CPA frequencies, simultaneously. The flexible tunabilities of the graphene metasurface-based CPA are of interests for tunable infrared detections and signal modulations.

Figure 10 shows the schematic of the proposed graphene nanoribbons-based metasurface and the corresponding excitation configuration with two counter-propagating and coherently modulated optical beams ($I_{\pm}$), $O_{\pm}$ being the respective output magnitudes; the graphene sheet is illuminated with perpendicularly polarized light. Both lattice constant and width of the graphene nanoribbon meta-atoms play important roles in determining the optical resonant

behaviors of graphene metasurface, the lattice constant is set to be $P=0.7$ μm for the study of CPA in the mid-infrared regime.

We took $E_F=0.5$ eV for the graphene. **Figure 11(a)** presents the spectra of the reflection coefficients (r) and transmission coefficients (t) for the case of graphene nanoribbon metasurface with the width of $w=0.33$ μm. We can see an obvious resonance around 23.0 THz. The resonance was confirmed to be electric dipolar mode (which will be verified from the effective surface conductivity below), similar to the low-frequency resonance of split ring resonators as that in reference [59]. The excitation of electric dipolar mode leads to the enhancement of absorption in the graphene sheet; however, the maximum limit is 50%.

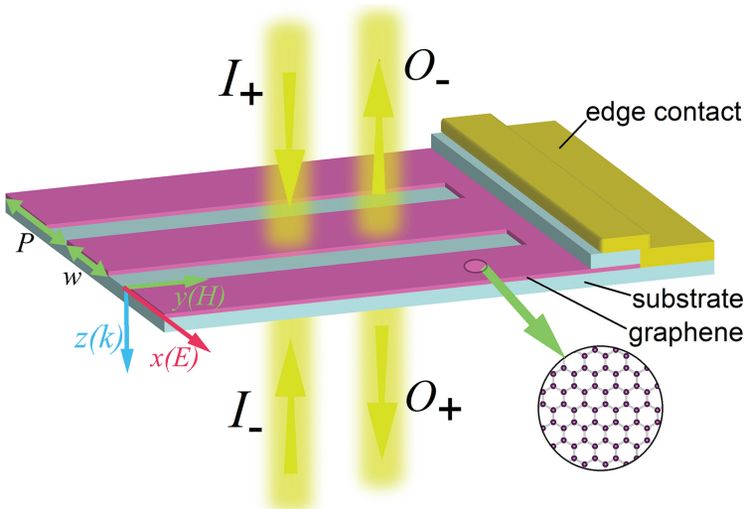

Figure 10. Schematic of a graphene ribbon metasurface illustrated by two counter-propagating and coherently modulated input beams.

Since the high-order scatterings of the deep subwavelength graphene nanoribbons are negligible, the graphene metasurface can be formalized with effective surface conductivities, then its interactions with the coherent modulated optical fields are the same as previously discussed suspending graphene case. The scatterings of the input beams are required to be inhibited to demonstrate a CPA, the necessary condition for CPA performance is $|t|=|r|$.

It can be seen from **Figure 11(a)** that there exists two frequencies (22.65 and 23.33 THz), which we call *quasi*-CPA points, which implies the necessary condition for suppressing the scattering fields to completely absorb coherent input beams of equal intensity. In the view of experiments, graphene generally needs to be transferred onto some substrate; we studied the scattering responses of a nanoribbon array (with the same geometry as that in **Figure 11(a)**) sandwiched in between two 45-nm-thick hexagonal boron nitride (h-BN) substrates, which was suggested as an exceptionally clean environment for achieving high confinement and low levels of plasmon damping in graphene [69] and is suitable for the one-dimensional high-quality electrical contact [70] (see the illustration in **Figure 10**). The dielectric function was taken from experimental studies [69, 71]. As can be seen from the inset of **Figure 11(a)**, the resonant frequency shifts to lower frequency as expected because of the introduction of the

substrate, and there exist two quasi-CPA frequencies. For simplicity and without loss of generality, we will consider free-standing graphene metasurfaces.

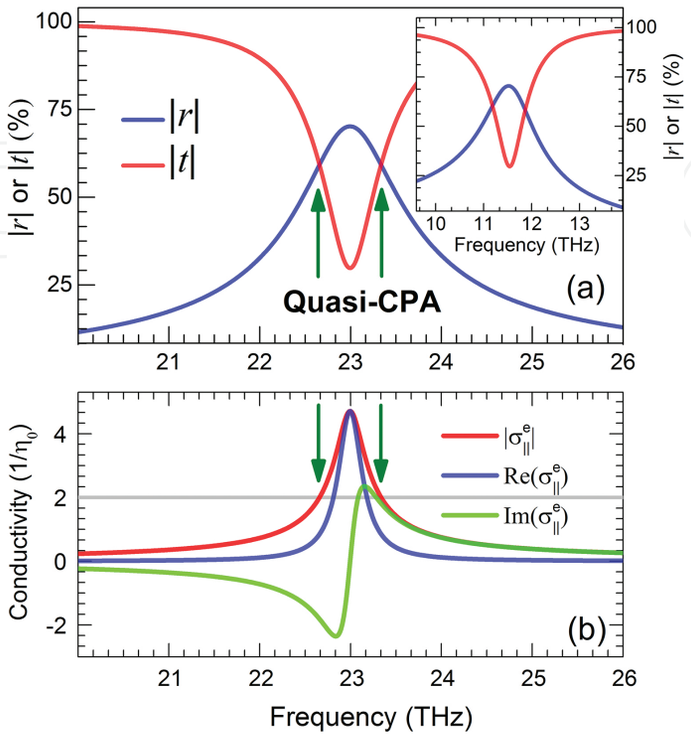

Figure 11. (a) Spectra of the reflection and transmission coefficients of a graphene nanoribbon metasurface; the quasi-CPA points at the crosses of the scattering spectra are indicated with arrows. (b) Absolute values, real and imaginary parts of the effective surface conductivities of the corresponding graphene nanoribbon metasurface.

Equation (**9**) gives the formation condition for CPA in an effective medium scheme. To verify this, we used a recently proposed sheet retrieval method (see Eq. (**3**)) to extract the effective surface conductivity $\sigma_{\parallel}^{e}$of the graphene nanoribbon metasurface. **Figure 11(b)** shows the absolute, real, and imaginary parts of the effective surface conductivities corresponding to **Figure 11(a)**. It is obvious that there is a Lorentz resonance around 23.0 THz on the effective electric conductivity spectrum, which confirms the excitation of electric dipolar mode. The extracted magnetic conductivity does not show any resonant feature around this electric resonance, so we have not included the corresponding result here. And it is also seen that the condition $|\sigma_{\parallel}^{e}\eta_0|=2$ is fulfilled at the two quasi-CPA frequencies, which indicate the validity of describing the graphene nanoribbon metasurface with the effective surface conductivity.

To implement the perfect absorption with the graphene metasurface, we set a chirped phase modulation $\Delta\phi(f)=\phi_+-\phi_-=\phi_0+kf$ on the beams $I_{\pm}$, with f being the frequency, and $k=-1.87\times10^{-12}\pi$ being the chirped factor to compensate the frequency dispersion. The plotted false-color map of the normalized spectra of total absorptions in **Figure 12(a)** shows the detailed dependence on ϕ_0. We see that a proper phase modulation (ϕ_0=1.03π) of the input coherent beams leads to significant suppression of the scattering outputs at the quasi-CPA

http://dx.doi.org/10.5772/64361

frequencies. The normalized total absorption as a function of the frequency for the phase modulation ϕ_0=1.03π is plotted in **Figure 12(b)**. We can see total absorption at both the two quasi-CPA frequencies. The significant boosting of the absorption implies destructive interference, which prevents the coherent beams from escaping the absorbing channel of the graphene metasurface, demonstrating completely absorption of the coherent input beams.

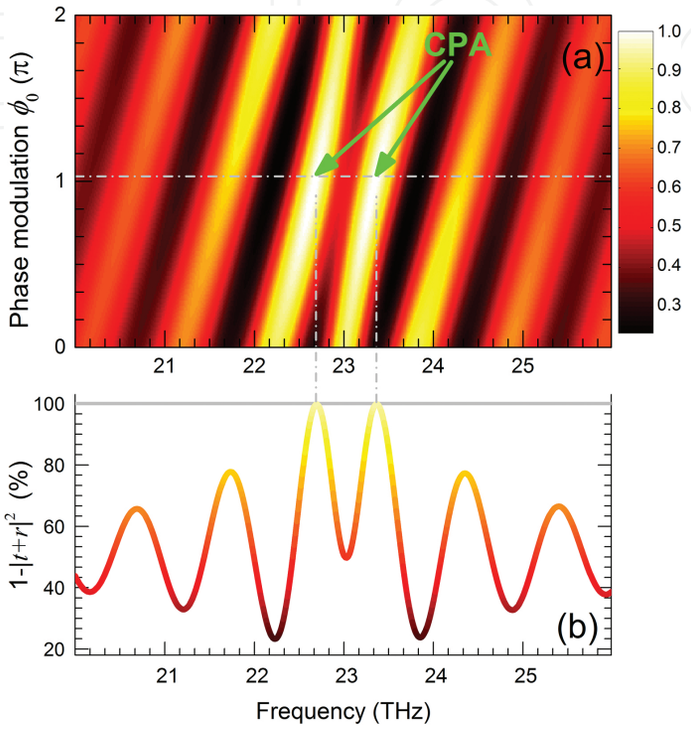

Figure 12. A two-dimensional false-color plot of the normalized total absorptions as a function of frequency and phase modulation, the exact CPA points are denoted with green arrows. (b) Normalized total absorption as a function of frequency for the phase modulation ϕ_0=1.03π.

The metasurface structures together with the electrically controlled graphene will provide more wide tunable space for the design of mid-infrared CPA; we first consider the geometric tunability of the graphene nanoribbon-based CPA. **Figure 13** shows the dependence of the difference ($|r|-|t|$) of the scattering coefficients of the graphene metasurface on the widths of nanoribbons. We can see that the resonant frequency of the electric dipolar mode shows a monotonous red shift with the increase of w, which is similar to the cut-wire case [60] (actually, the ribbon structure is the special situation of cut-wire with graphene covering all the lattice range along the x-axis). Increasing the width or the graphene-filling factor in the unit cell of the metasurface leads to stronger light-graphene interaction, that is, high resonant strength of the electric dipolar resonance, and thus higher r and lower t around the resonance that introduce a regime where $|r|-|t|=0$ starting from w=0.138 μm, which has its boundary (as the solid line indicated) being the quasi-CPA points. The discrete spheres on top of the solid curve, representing the extracted surface conductivities with $|\sigma_{\parallel}^{e}\eta_0|=2$, also imply that the formation condition of CPA is fulfilled at the boundary. At these quasi-CPA points, we can

completely suppress the scatterings of the graphene metasurface with proper phase modulations as that shown in **Figure 12**.

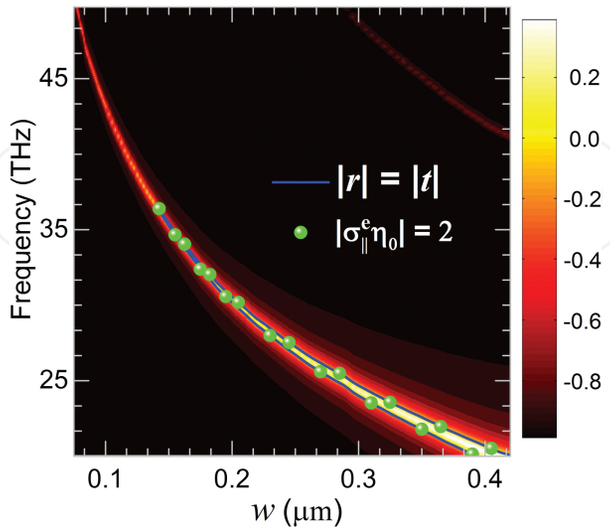

Figure 13. Geometric tunability of the graphene metasurface CPA.

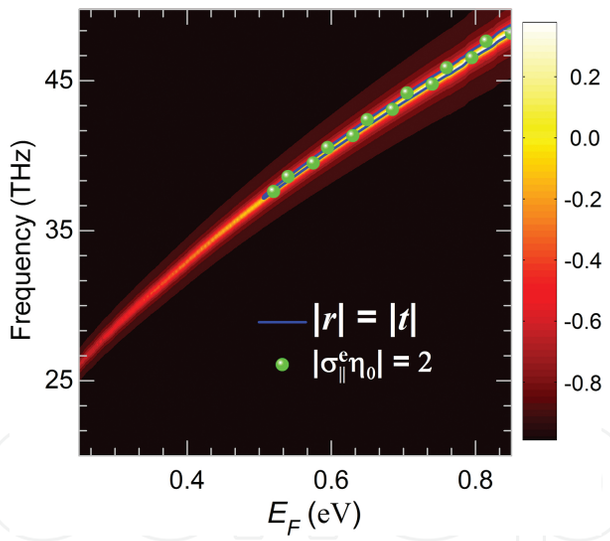

Figure 14. Electric tunability of the graphene metasurface CPA.

On the other hand, the graphene metasurface is also expected to have higher resonant strength for graphene with larger Fermi level. The dependence on Fermi energy of the difference of the scattering coefficients is plotted in **Figure 14** (the width of the graphene nanoribbon was set to be 0.138 μm, the left edge of the solid boundary in **Figure 13**); it can be seen that the resonant frequency shifts to higher frequencies and the resonant strength becomes higher while the Fermi level changes from0.25 to 0.85 eV. Similar to the influence of the width of nanoribbons, the light-graphene interaction is enhanced for better resonant behaviors, and thus a regime

starting from 0.5 eV where with its boundary $|t|-|r|=0$ being the quasi-CPA frequencies. Combining the two functional bands for CPA, we see that it is free to achieve CPA at desired frequency in an ultra-wide range by merging the geometric and electrical tunabilities. And the discrete spheres representing the extracted surface conductivities in **Figure 14** again confirm that $|\sigma_{\|}^{e}\eta_0|=2$ is equivalent to the quasi-CPA condition $|t|=|r|$ for graphene nanoribbons-based metasurface.

4. Conclusion

In summary, this chapter summarized the recent progresses in the subfield of graphene plasmonics. Aimed to the issue in practical applications based on graphene: high loss in the plasmonic excitations of graphene limits the performance of graphene's ability in manipulating light. We show some reported results on the enhancement of light-graphene interactions by employing the new strategies including plasmonic metamaterial design and coherent modulation on optical fields. We found that the terahertz/ infrared extinction and absorption can be enhanced in a single graphene sheet by patterning plasmonic metamaterial structures, such as SRRs and cut-wires. It is found that we can significantly control the plasmonic excitations by manipulating geometric symmetry. It is shown that the electric plasmonic mode is stronger in enhancing infrared extinction and absorption compared to the magnetic mode and higher-order modes. We prove that the condition for maximum 50% absorption is $\sigma_r\eta_0=2$. It is also found that graphene metamaterials interacting with coherent-modulated optical fields can be employed to further take advantages from plasmonic excitations in infrared frequencies to perfectly suppress scattering for CPA. We prove that the necessary condition for realizing CPA for both suspending graphene and graphene metamaterial cases is $|\sigma\eta_0|=2$. Furthermore, the CPA can be tuned in an ultra-wide frequency band by considering both the geometric tunability and electrically controlled charge-carrier density in graphene. Our results on enhancing optical response in graphene with plasmonic metamaterial design, coherent modulations, and synergic action of them have potential applications for terahertz and infrared band graphene photonics and optoelectronics. We also expect potential applications of plasmonic metamaterial design and coherent modulations in two-dimensional materials beyond graphene.

Acknowledgements

Y. Fan would like to acknowledge Prof. C. M. Soukoulis, Prof. Q. Zhao, Dr. N.-H. Shen, and Mr. P. Zhang for collaboration and helpful discussion. This work was supported by the NSFC (Grant Nos. 11674266, 61505164 and 11372248), the Program for Scientific Activities of Selected Returned Overseas Professionals in Shaanxi Province, the Fundamental Research Funds for the Central Universities (Grant Nos. 3102015ZY079 and 3102015ZY058), and the Shaanxi Project for Young New Star in Science and Technology (Grant No. 2015KJXX-11).

Author details

Yuancheng Fan[1*], Fuli Zhang[1], Quanhong Fu[1] and Hongqiang Li[2]

*Address all correspondence to: phyfan@nwpu.edu.cn

1 Department of Applied Physics, School of Science, Northwestern Polytechnical University, Xi'an, China

2 The Institute of Dongguan–Tongji University, Dongguan, Guangdong, China

References

[1] Novoselov KS, Geim AK, Morozov SV, Jiang D, Zhang Y, Dubonos SV, Grigorieva IV, Firsov AA. Electric field effect in atomically thin carbon films. Science. 2004;306(5696): 666–669. DOI: 10.1126/science.1102896.

[2] Geim AK, Novoselov KS. The rise of graphene. Nat. Mater. 2007;6(3):183–191. DOI: 10.1038/nmat1849.

[3] Butler SZ, Hollen SM, Cao LY, Cui Y, Gupta JA, Gutierrez HR, Heinz TF, Hong SS, Huang JX, Ismach AF, Johnston-Halperin E, Kuno M, Plashnitsa VV, Robinson RD, Ruoff RS, Salahuddin S, Shan J, Shi L, Spencer MG, Terrones M, Windl W, Goldberger JE. Progress, challenges, and opportunities in two-dimensional materials beyond graphene. ACS Nano. 2013;7(4):2898–2926. DOI: 10.1021/nn400280c.

[4] Fiori G, Bonaccorso F, Iannaccone G, Palacios T, Neumaier D, Seabaugh A, Banerjee SK, Colombo L. Electronics based on two-dimensional materials. Nat. Nanotechnol. 2014;9(12):1063–1063. DOI: 10.1038/nnano.2014.283.

[5] Morozov SV, Novoselov KS, Katsnelson MI, Schedin F, Elias DC, Jaszczak JA, Geim AK. Giant intrinsic carrier mobilities in graphene and its bilayer. Phys. Rev. Lett. 2008;100(1). DOI: 10.1103/PhysRevLett.100.016602[1–4].

[6] Lee C, Wei XD, Kysar JW, Hone J. Measurement of the elastic properties and intrinsic strength of monolayer graphene. Science. 2008;321(5887):385–388. DOI: 10.1126/science.1157996.

[7] Balandin AA, Ghosh S, Bao WZ, Calizo I, Teweldebrhan D, Miao F, Lau CN. Superior thermal conductivity of single-layer graphene. Nano Lett. 2008;8(3):902–907. DOI: 10.1021/nl0731872.

[8] Bonaccorso F, Sun Z, Hasan T, Ferrari AC. Graphene photonics and optoelectronics. Nat. Photonics. 2010;4(9):611–622. DOI: 10.1038/nphoton.2010.186.

[9] de Abajo FJG. Graphene plasmonics: challenges and opportunities. ACS Photonics. 2014;1(3):135–152. DOI: 10.1021/ph400147y.

[10] Yan H, Li X, Chandra B, Tulevski G, Wu Y, Freitag M, Zhu W, Avouris P, Xia F. Tunable infrared plasmonic devices using graphene/insulator stacks. Nat. Nanotechnol. 2012;7:330–334. DOI: 10.1038/nnano.2012.59.

[11] Jablan M, Buljan H, Soljacic M. Plasmonics in graphene at infrared frequencies. Phys. Rev. B. 2009;80(24). DOI: 10.1103/PhysRevB.80.245435[1–7].

[12] Chen J, Badioli M, Alonso-Gonzalez P, Thongrattanasiri S, Huth F, Osmond J, Spasenovic M, Centeno A, Pesquera A, Godignon P, Zurutuza Elorza A, Camara N, Javier Garcia de Abajo F, Hillenbrand R, Koppens FHL. Optical nano-imaging of gate-tunable graphene plasmons. Nature. 2012;487(7405):77–81. DOI: 10.1038/nature11254.

[13] Fei Z, Rodin AS, Andreev GO, Bao W, McLeod AS, Wagner M, Zhang LM, Zhao Z, Thiemens M, Dominguez G, Fogler MM, Castro Neto AH, Lau CN, Keilmann F, Basov DN. Gate-tuning of graphene plasmons revealed by infrared nano-imaging. Nature. 2012;487(7405):82–85. DOI: 10.1038/nature11253.

[14] Gerber JA, Berweger S, O'Callahan BT, Raschke MB. Phase-resolved surface plasmon interferometry of graphene. Phys. Rev. Lett. 2014;113(5). DOI: 10.1103/PhysRevLett.113.055502[1–5].

[15] Vakil A, Engheta N. Transformation optics using graphene. Science. 2011;332(6035):1291–1294. DOI: 10.1126/science.1202691.

[16] Koppens FHL, Chang DE, de Abajo FJG. Graphene plasmonics: a platform for strong light-matter interactions. Nano Lett. 2011;11(8):3370–3377. DOI: 10.1021/nl201771h.

[17] Wang F, Zhang YB, Tian CS, Girit C, Zettl A, Crommie M, Shen YR. Gate-variable optical transitions in graphene. Science. 2008;320(5873):206–209. DOI: 10.1126/science.1152793.

[18] Li ZQ, Henriksen EA, Jiang Z, Hao Z, Martin MC, Kim P, Stormer HL, Basov DN. Dirac charge dynamics in graphene by infrared spectroscopy. Nat. Phys. 2008;4(7):532–535. DOI: 10.1038/nphys989.

[19] Horng J, Chen CF, Geng BS, Girit C, Zhang YB, Hao Z, Bechtel HA, Martin M, Zettl A, Crommie MF, Shen YR, Wang F. Drude conductivity of Dirac fermions in graphene. Phys. Rev. B. 2011;83(16). DOI: 10.1103/PhysRevB.83.165113[1–5].

[20] Tassin P, Koschny T, Soukoulis CM. Graphene for terahertz applications. Science. 2013;341(6146):620–621. DOI: 10.1126/science.1242253.

[21] Kane CL, Mele EJ. Quantum spin Hall effect in graphene. Phys. Rev. Lett. 2005;95(22). DOI: 10.1103/PhysRevLett.95.226801[1–4].

[22] Yao YG, Ye F, Qi XL, Zhang SC, Fang Z. Spin-orbit gap of graphene: First-principles calculations. Phys. Rev. B. 2007;75(4). DOI: 10.1103/PhysRevB.75.041401[1–4].

[23] Zhang ZR, Li HQ, Gong ZJ, Fan YC, Zhang TQ, Chen H. Extend the omnidirectional electronic gap of Thue-Morse aperiodic gapped graphene superlattices. Appl. Phys. Lett. 2012;101(25). DOI: 10.1063/1.252104[1–4].

[24] Engheta N. Circuits with light at nanoscales: Optical nanocircuits inspired by metamaterials. Science. 2007;317(5845):1698–1702. DOI: 10.1126/science.1133268.

[25] Fan YC, Han J, Wei ZY, Wu C, Cao Y, Yu X, Li HQ. Subwavelength electromagnetic diode: One-way response of cascading nonlinear meta-atoms. Appl. Phys. Lett. 2011;98(15). DOI: 10.1063/1.151903[1–3].

[26] Fan YC, Wei ZY, Han J, Liu XG, Li HQ. Nonlinear properties of meta-dimer comprised of coupled ring resonators. J. Phys. D-Appl. Phys. 2011;44(42). DOI: 10.1088/0022-3727/44/42/425303[1–4].

[27] Yablonovitch E. Inhibited spontaneous emission in solid-state physics and electronics. Phys. Rev. Lett. 1987;58(20):2059–2062. DOI: 10.1103/PhysRevLett.58.2059.

[28] Smith DR, Pendry JB, Wiltshire MCK. Metamaterials and negative refractive index. Science. 2004;305(5685):788–792. DOI: 10.1126/science.1096796.

[29] Soukoulis CM, Wegener M. Past achievements and future challenges in the development of three-dimensional photonic metamaterials. Nat. Photonics. 2011;5(9):523–530. DOI: 10.1038/nphoton.2011.154.

[30] Gan X, Shiue R-J, Gao Y, Mak KF, Yao X, Li L, Szep A, Walker D, Hone J, Heinz TF, Englund D. High-contrast electrooptic modulation of a photonic crystal nanocavity by electrical gating of graphene. Nano Lett. 2013;13:691–696. DOI: 10.1021/nl304357u.

[31] Piper JR, Fan S. Total absorption in a graphene monolayer in the optical regime by critical coupling with a photonic crystal guided resonance. ACS Photonics. 2014;1:347–353. DOI: 10.1021/ph400090p.

[32] Gu T, Andryieuski A, Hao Y, Li Y, Hone J, Wong CW, Lavrinenko A, Low T, Heinz TF. Photonic and plasmonic guided modes in graphene–silicon photonic crystals. ACS Photonics. 2015;2:1552–1558. DOI: 10.1021/acsphotonics.5b00209.

[33] Zheng J, Barton RA, Englund D. Broadband coherent absorption in chirped-planar-dielectric cavities for 2D-material-based photovoltaics and photodetectors. ACS Photonics. 2014;1:768–774. DOI: 10.1021/ph500107b.

[34] Fan YC, Wei ZY, Li HQ, Chen H, Soukoulis CM. Photonic band gap of a graphene-embedded quarter-wave stack. Phys. Rev. B. 2013;88(24). DOI: 10.1103/PhysRevB.88.241403[1–5].

[35] Liu N, Guo HC, Fu LW, Kaiser S, Schweizer H, Giessen H. Three-dimensional photonic metamaterials at optical frequencies. Nat. Mater. 2008;7(1):31–37. DOI: 10.1038/nmat2072.

[36] Zhang FL, Zhao Q, Kang L, Zhou J, Lippens D. Experimental verification of isotropic and polarization properties of high permittivity-based metamaterial. Phys. Rev. B. 2009;80(19). DOI: 10.1103/PhysRevB.80.195119[1–6].

[37] Wei ZY, Cao Y, Han J, Wu C, Fan YC, Li HQ. Broadband negative refraction in stacked fishnet metamaterial. Appl. Phys. Lett. 2010;97(14). DOI: 10.1063/1.141901[1–3].

[38] Han J, Li HQ, Fan YC, Wei ZY, Wu C, Cao Y, Yu X, Li F, Wang ZS. An ultrathin twist-structure polarization transformer based on fish-scale metallic wires. Appl. Phys. Lett. 2011;98(15). DOI: 10.1063/1.151908[1–3].

[39] Wei ZY, Cao Y, Fan YC, Yu X, Li HQ. Broadband polarization transformation via enhanced asymmetric transmission through arrays of twisted complementary split-ring resonators. Appl. Phys. Lett. 2011;99(22). DOI: 10.1063/1.221907[1–3].

[40] Wei ZY, Cao Y, Fan YC, Yu X, Li HQ. Broadband transparency achieved with the stacked metallic multi-layers perforated with coaxial annular apertures. Opt. Express. 2011;19(22):21425–21431. DOI: 10.1364/oe.19.021425.

[41] Zhang FL, Zhao Q, Zhou J, Wang SX. Polarization and incidence insensitive dielectric electromagnetically induced transparency metamaterial. Opt. Express. 2013;21(17): 19675–19680. DOI: 10.1364/oe.21.019675.

[42] Zhang FL, Feng SQ, Qiu KP, Liu ZJ, Fan YC, Zhang WH, Zhao Q, Zhou J. Mechanically stretchable and tunable metamaterial absorber. Appl. Phys. Lett. 2015;106(9). DOI: 10.1063/1.091907[1–5].

[43] Yu N, Capasso F. Flat optics with designer metasurfaces. Nat. Mater. 2014;13(2):139–150. DOI: 10.1038/nmat3839.

[44] Kildishev AV, Boltasseva A, Shalaev VM. Planar photonics with metasurfaces. Science. 2013;339(6125). DOI: 10.1126/science.1232009[1–6].

[45] Yu NF, Genevet P, Kats MA, Aieta F, Tetienne JP, Capasso F, Gaburro Z. Light propagation with phase discontinuities: generalized laws of reflection and refraction. Science. 2011;334(6054):333–337. DOI: 10.1126/science.1210713.

[46] Ni XJ, Emani NK, Kildishev AV, Boltasseva A, Shalaev VM. Broadband light bending with plasmonic nanoantennas. Science. 2012;335(6067):427–427. DOI: 10.1126/science.1214686.

[47] Sun SL, He Q, Xiao SY, Xu Q, Li X, Zhou L. Gradient-index meta-surfaces as a bridge linking propagating waves and surface waves. Nat. Mater. 2012;11(5):426–431. DOI: 10.1038/nmat3292.

[48] Yin XB, Ye ZL, Rho J, Wang Y, Zhang X. Photonic spin Hall effect at metasurfaces. Science. 2013;339(6126):1405–1407. DOI: 10.1126/science.1231758.

[49] Shitrit N, Yulevich I, Maguid E, Ozeri D, Veksler D, Kleiner V, Hasman E. Spin-optical metamaterial route to spin-controlled photonics. Science. 2013;340(6133):724–726. DOI: 10.1126/science.1234892.

[50] Chong YD, Ge L, Cao H, Stone AD. Coherent perfect absorbers: Time-reversed lasers. Phys. Rev. Lett. 2010;105(5). DOI: 10.1103/PhysRevLett.105.053901[1–4].

[51] Wan WJ, Chong YD, Ge L, Noh H, Stone AD, Cao H. Time-reversed lasing and interferometric control of absorption. Science. 2011;331(6019):889–892. DOI: 10.1126/science.1200735.

[52] Longhi S. PT-symmetric laser absorber. Phys. Rev. A. 2010;82(3). DOI: 10.1103/PhysRevA.82.031801[1 –4].

[53] Lin Z, Ramezani H, Eichelkraut T, Kottos T, Cao H, Christodoulides DN. Unidirectional invisibility induced by PT-symmetric periodic structures. Phys. Rev. Lett. 2011;106(21). DOI: 10.1103/PhysRevLett.106.213901[1–4].

[54] Noh H, Chong YD, Stone AD, Cao H. Perfect coupling of light to surface plasmons by coherent absorption. Phys. Rev. Lett. 2012;108(18). DOI: 10.1103/PhysRevLett.108.186805[1–5].

[55] Crescimanno M, Dawson NJ, Andrews JH. Coherent perfect rotation. Phys. Rev. A. 2012;86(3). DOI: 10.1103/PhysRevA.86.031807[1–4].

[56] Zhang J, MacDonald KF, Zheludev NI. Controlling light-with-light without nonlinearity. Light-Sci. Appl. 2012;1. DOI: 10.1038/lsa.2012.18[1–5].

[57] Hao JM, Zhou L, Qiu M. Nearly total absorption of light and heat generation by plasmonic metamaterials. Phys. Rev. B. 2011;83(16). DOI: 10.1103/PhysRevB.83.165107[1–12].

[58] Pu MB, Feng Q, Hu CG, Luo XG. Perfect absorption of light by coherently induced plasmon hybridization in ultrathin metamaterial film. Plasmonics. 2012;7(4):733–738. DOI: 10.1007/s11468-012-9365-1.

[59] Fan YC, Wei ZY, Zhang ZR, Li HQ. Enhancing infrared extinction and absorption in a monolayer graphene sheet by harvesting the electric dipolar mode of split ring resonators. Opt. Lett. 2013;38(24):5410–5413. DOI: 10.1364/ol.38.005410.

[60] Fan YC, Shen NH, Koschny T, Soukoulis CM. Tunable terahertz meta-surface with graphene cut-wires. ACS Photonics. 2015;2(1):151–156. DOI: 10.1021/ph500366z.

[61] Fan YC, Zhang FL, Zhao Q, Wei ZY, Li HQ. Tunable terahertz coherent perfect absorption in a monolayer graphene. Opt. Lett. 2014;39(21):6269–6272. DOI: 10.1364/ol.39.006269.

[62] Fan Y, Liu Z, Zhang F, Zhao Q, Wei Z, Fu Q, Li J, Gu C, Li H. Tunable mid-infrared coherent perfect absorption in a graphene meta-surface. Sci. Reports. 2015;5. DOI: 10.1038/srep13956[1–8].

[63] Fedotov VA, Rose M, Prosvirnin SL, Papasimakis N, Zheludev NI. Sharp trapped-mode resonances in planar metamaterials with a broken structural symmetry. Phys. Rev. Lett. 2007;99(14). DOI: 10.1103/PhysRevLett.99.147401[1–4].

[64] Al-Naib IAI, Jansen C, Koch M. High Q-factor metasurfaces based on miniaturized asymmetric single split resonators. Appl. Phys. Lett. 2009;94(15). DOI: 10.1063/1.153505[1–3].

[65] Fan YC, Wei ZY, Li HQ, Chen H, Soukoulis CM. Low-loss and high-Q planar metamaterial with toroidal moment. Phys. Rev. B. 2013;87(11). DOI: 10.1103/PhysRevB.87.115471[1–5].

[66] Smith DR, Schultz S, Markos P, Soukoulis CM. Determination of effective permittivity and permeability of metamaterials from reflection and transmission coefficients. Phys. Rev. B. 2002;65(19). DOI: 10.1103/PhysRevB.65.195104[1–5].

[67] Chen XD, Grzegorczyk TM, Wu BI, Pacheco J, Kong JA. Robust method to retrieve the constitutive effective parameters of metamaterials. Phys. Rev. E. 2004;70(1). DOI: 10.1103/PhysRevE.70.016608[1–7].

[68] Tassin P, Koschny T, Soukoulis C. Effective material parameter retrieval for thin sheets: Theory and application to graphene, thin silver films, and single-layer metamaterials. Phys. B. 2012;407(20):4062–4065. DOI: 10.1016/j.physb.2012.01.119.

[69] Woessner A, Lundeberg MB, Gao Y, Principi A, Alonso-Gonzaolez P, Carrega M, Watanabe K, Taniguchi T, Vignale G, Polini M, Hone J, Hillenbrand R, Koppens FHL. Highly confined low-loss plasmons in graphene-boron nitride heterostructures. Nat. Mater. 2015;14(4):421–425. DOI: 10.1038/nmat4169.

[70] Wang L, Meric I, Huang PY, Gao Q, Gao Y, Tran H, Taniguchi T, Watanabe K, Campos LM, Muller DA, Guo J, Kim P, Hone J, Shepard KL, Dean CR. One-dimensional electrical contact to a two-dimensional material. Science. 2013;342(6158):614–617. DOI: 10.1126/science.1244358.

[71] Caldwell JD, Kretinin AV, Chen Y, Giannini V, Fogler MM, Francescato Y, Ellis CT, Tischler JG, Woods CR, Giles AJ, Hong M, Watanabe K, Taniguchi T, Maier SA, Novoselov KS. Sub-diffractional volume-confined polaritons in the natural hyperbolic material hexagonal boron nitride. Nat. Commun. 2014;5. DOI: 10.1038/ncomms5221[1–9].

IntechOpen